## Reviewer #1 Evaluation:

We thank the reviewer for their thorough evaluation and constructive feedback on our manuscript. Based on this, we propose several changes below that we believe address the reviewers' concerns and improve the manuscript. These changes are summarized in this letter, along with specific responses to the reviewers' comments. Below the reviewer's comments our response is shown in **bold**. Proposed modifications and / or additions to the manuscript are shown in *italics*.

Prior to the start of EISCAT_3D radar observations, this paper shows how the accuracy of the ionospheric potential reconstruction changes by varying the beam pattern of the EISCAT_3D radar. It deserves publication with some minor modifications, as this is a very important toolkit needed when designing experiments according to the scientific objectives of each user.

**Thank you! We have strived to bring the manuscript and our responses here in line with recommendations from both reviewers.**

Minor revisions:

Figures 4g-i: The scatter plots are used to show that the accuracy of the estimation results is good, but information on where the residuals are small is lost if only the scatter plots are used. It is therefore recommended that the scatterplot is replaced or added to a two-dimensional heatmap displaying the residuals of the estimates for GEMINI.

**We agree that the scatter plots make it difficult to see where the residuals are small. On the other hand, after trying various strategies we also find it difficult to visually indicate where the residuals are small without significantly expanding Figure 4. We propose to instead present these results as heatmaps in Figure S2, shown below, which will be located in a new Supplement along with the following text:**

> *Figure S2 shows heatmaps of original versus reconstructed eastward (d–f), northward (g–i), and upward (j–l) velocity components for the three beam patterns shown in Figure 4. These heatmaps indicate that for all beam patterns the reconstructed convection velocities are generally within a few tens of m/s of the original convection velocities. Differences between the various beam patterns are mostly negligible but nevertheless visible.*
>
> *Results in this figure reinforce the conclusion in the main manuscript that the goal of the second example experiment in Section 5.2 (reconstruction of the ionospheric convection pattern with as little overall residual error as possible) is approximately equally well achieved by all three beam patterns.*

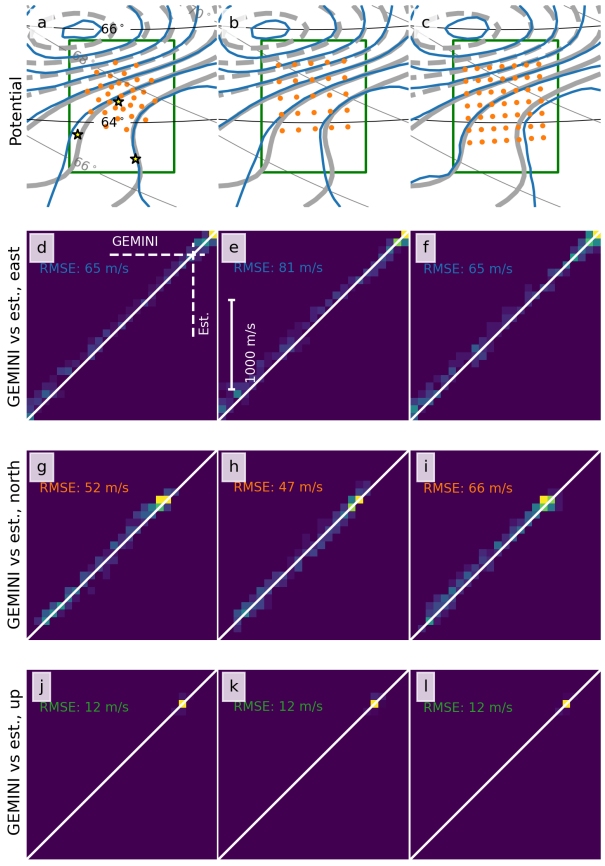


**Proposed caption for new Figure S2 in supplement:** Reconstruction of ionospheric potential for the three different beam patterns shown in Figure 4 (from left to right): the Reistad et al (2024) beam pattern, and 25- and 47-beam patterns covering respectively ~160 km² and ~180 km².
a–c: Original and reconstructed ionospheric potential patterns (thick gray lines and thin blue lines, respectively), identical to those shown in Figures 4a–c in the main article.
d–f: Reconstructed eastward convection plotted against true convection y and x axes, respectively).
g–i: Reconstructed northward convection plotted against true convection.
j–l: Reconstructed upward convection plotted against true convection.

Equation (6): Definition of "N" should be added.

**We propose to change the sentence just prior to Equation 6 so that it now reads** "*Thus the set of N measurements of the ACF at time lag τ with scattering vector* ***k*** *is represented by the measurement vector […]*".

Equation (10): It is suggested that a more detailed explanation of formula conversions be added, in addition to citing references, to make it easier for the reader to understand.

**We agree that more details are needed here, thank you for pointing this out. We propose to rewrite a large portion of the text following Equation 10 to describe in detail how we use Equation 10 in practice. We also propose to add several details about the uncertainty estimation process, which we hope the reviewer will agree makes the actual procedure easier for the reader to understand.**

**The following image contains our proposed rewrite of this section.**

### 2.3 Uncertainty estimation procedure

At the highest level, our uncertainty estimation procedure consists of two steps: estimation of the ACF measurement error covariance matrix $\mathbf{\Sigma}_m$, and plasma parameter uncertainty estimation via Equation 9.

In the first step we estimate the ACF measurement covariance matrix $\mathbf{\Sigma}_m$ as follows. We assume that measurements of the ACF at different lags are uncorrelated and have the same variance $\sigma^2$, so that $\mathbf{\Sigma}_m$ is an identity matrix multiplied by $\sigma^2$. With these assumptions, the ACF noise level may be defined as (Vallinkoski, 1988)

$$\gamma^2 = \frac{\sigma^2}{f(\mathbf{k}, 0; \mathbf{x})^2 N_\tau} = \frac{N_a}{N_\tau} \frac{1}{\mathrm{SNR}^2}, \tag{10}$$

with $N_a$ the number of averaged ACF samples, $N_\tau \approx 2\pi/(\omega_0 \Delta\tau)$ the approximate number of lags to the first zero of the ACF assuming zero plasma bulk flow, $\omega_0 = k\sqrt{2k_B T_i/m_i}$ the "ion angular Doppler frequency" (Vallinkoski, 1988) for scattering wave number $k$, and $\Delta\tau = 2\Delta r/c$ the lag spacing (sampling interval) of ACF measurements. The lag spacing is matched with the user-specified range resolution $\Delta r$. The number $N_a$ accounts for the number of samples averaged in phase-code decoding, as well as post-integration in range and time.

With this definition, we calculate the SNR and the ACF noise level at each site as described in Section 2.1 using the radar equation assuming a particular set of radar system parameters, and assuming Gaussian beam shapes and pulse shapes. (See Sections B.3–B.6 in Lehtinen et al., 2014, as well as the routine "`multistaticNoiseLevels`" in Virtanen, 2023.) The outputs from this step are the separate ACF noise levels $\gamma_s$ for each transmitter-receiver pair $s$.

In the second step (plasma parameter uncertainty estimation) we use the fact that uncertainty of the line-of-sight velocity $v_i$ is practically independent of the errors of the other parameters, and assume that all receivers see the same $n_e$, $T_e$, and $T_i$. The latter assumption is equivalent to assuming that $T_e$ and $T_i$ are isotropic. (In reality $T_e$ and $T_i$ may be neither isotropic nor equal; see discussion in, e.g., Virtanen et al., 2014, and references therein.) The uncertainty estimation itself can therefore be divided into two parts: calculation of (i) the variance of estimates of scalar parameters, which do not have a direction, and (ii) the covariance of ion drift velocity vector estimates.

To calculate (i) we simply sum information from all receivers (since information or precision is the inverse of variance) to get a combined ACF noise level for the full multistatic system: $\gamma = \left(\sum_s \gamma_s^{-2}\right)^{-1/2}$. We then calculate the theoretical ACF $f(\mathbf{k}, \tau = 0; \mathbf{x})$, and solve for the ACF variance $\sigma^2$ in Equation 10 (see routines "`parameterFitErrors`" and "`ISspectrumSimple`" in Virtanen, 2023). We thus have an estimate of the ACF covariance matrix $\mathbf{\Sigma}_m$. We then calculate the theory matrix $\mathbf{A}$, and finally calculate the posterior model covariance matrix in Equation 9, with the scalar plasma parameter uncertainties taken to be the square roots of its diagonal elements.

To calculate (ii) one must consider the system geometry, and in general the estimate of the line-of-sight ion drift for each transmitter-receiver pair has a different uncertainty. We combine the different uncertainties following the methodology outlined in Appendix B. For a monostatic system the ion drift velocity covariance matrix reduces to a scalar representing the variance of the line-of-sight ion velocity.

Line 173: It is helpful for readers to add more detailed explanation about B.2.4 of Lehtinen et al. (2014).

**We propose to include in the revised manuscript a new Appendix B that gives a full description of the procedure we use. The text of the proposed Appendix B is contained in the following image:**

**Appendix B: Velocity covariance matrix estimation**

We use the following procedure to obtain the velocity covariance matrix from estimates of the line-of-sight velocity from multiple transmitter-receiver pairs. It is taken directly from Section B.2.4 of Lehtinen et al. (2014).

Given the true velocity vector $\mathbf{v} = (v_x, v_y, v_z)^T$ and the scattering wave unit vector $\hat{\mathbf{k}}_s = \frac{1}{\|\mathbf{k}_s\|}(k_{sx}, k_{sy}, k_{sz})^T$ at site $s$, the line-of-sight velocity at site $s$ is

$$v_s = \frac{1}{\|\mathbf{k}_s\|}(v_x k_{sx} + v_y k_{sy} + v_z k_{sz}). \tag{B1}$$

With line-of-sight velocity estimates from all $N_s$ radar transmitter-receiver pairs, we have

$$(v_1, v_2, \ldots, v_{N_s})^T = \mathbf{A}_v \cdot \mathbf{v} + (\epsilon_1, \epsilon_2, \ldots, \epsilon_{N_s})^T, \tag{B2}$$

where

$$\mathbf{A}_v = \left(\hat{\mathbf{k}}_1 \quad \hat{\mathbf{k}}_2 \quad \ldots \quad \hat{\mathbf{k}}_{N_s}\right)^T. \tag{B3}$$



and $\epsilon_s$ is the uncertainty of the line-of-sight velocity estimate at site $s$. The corresponding a posteriori covariance matrix of the full velocity vector is

$$\Sigma_{pv} = \left(\mathbf{A}_v^T \mathbf{\Sigma}_v^{-1} \mathbf{A}_v\right)^{-1}. \tag{B4}$$

Line 201–202: Why were uncertainties estimated by this study underestimated relative to those of GUISDAP above ~300-km altitudes? Are assumptions used in GUISDAP desirable compared to e3doubt?

**This is a reasonable question that is unfortunately not easy to answer. Our combined experience with GUISDAP is that the code is opaque, and documentation of the exact assumptions that GUISDAP makes is, to our knowledge, nowhere publicly available.**

**Two points that may be worth raising are the following.**

**1. Both GUISDAP and our uncertainty estimation procedure (e3doubt) allow for variable range resolution as a function of altitude. For this particular experiment the range resolution was generally less than 5 km below 120-km altitude, less than 10 km below 160-km altitude, and between 10 and 30 km above 160-km altitude. Uncertainty decreases with decreasing spatial resolution (i.e., larger range resolution).**

**2. GUISDAP has an option for modeling error correlations that increases the computational cost of the calculations by a factor of approximately $10^4$, making use of this option impractical for the vast majority of analysis. However, one of us (IV) has investigated and found that inclusion of error correlation effects quite precisely creates the approximate factor-of-two difference between GUISDAP uncertainty estimates and the sample standard deviations shown in Figure 2.**

**In the revised manuscript we can make the point about variable range resolution and slightly expand the discussion of error correlation if the reviewer agrees that these points are informative.**

Line 314: The abbreviation "SECS" should be added after "spherical elementary current system".
Line 331: "Madelaire et al. (2023)" should be "(Madelaire et al., 2023)".
Line 345: "(Reistad et al., 2024)" should be "Reistad et al. (2024)".

**We will correct all of these in the revised manuscript. Thank you for catching these mistakes.**